Proceedings of the Defence and Security Conference
Vol. 1, No. 1, pp. 426-440, 4 April 2025.
Category: Original scientific paper

ATOMIC FORCE MICROSCOPY: TOPOGRAPHY ANALYSIS OF GRENADE BODY

Andrej Razumić[1], Zvonko Trzun[2], Zdravko Jakop[3], Marin Kurtela[4], Biserka Runje[5]

[1,2,3]Dr. Franjo Tuđman Defense and Security University
E-mails: andrej.razumic@sois-ft.hr, zvonko.trzun@sois-ft.hr, zdravko.jakop@sois-ft.hr

[4,5]University of Zagreb / Faculty of Mechanical Engineering and Naval Architecture
E-mails: marin.kurtela@fsb.unizg.hr, biserka.runje@fsb.unizg.hr

Abstract

Grenades are projectiles that can be either guided or unguided and are employed in military and ballistic applications to neutralise targets at varying distances. Their construction and surface treatment are critical for optimising performance, including accuracy, precision, durability, and aerodynamic properties. The surface topography of the grenade body plays a significant role, as it affects the structural resistance of the material, friction and wear during passage through the barrel, as well as aerodynamic properties and flight stability, all of which collectively determine the grenade's precision, range, and effectiveness upon target impact. In this study, the surface topography of the Shell 155 body was analysed using atomic force microscopy (AFM). AFM operates on the principle of scanning the sample surface with a nanoscale sharp-tipped probe. The study examined the surface quality of grenade bodies with three different surface protection methods: powder coating, adonisation, and hard anodisation. The results include areal topography parameters and 2D and 3D visualisations of the grenade body surface.

Keywords: grenade, surface topography, atomic force microscopy, Shell 155

1. INTRODUCTION

Grenades are artillery projectiles with high-explosive charges (Hrvatska enciklopedija, 2025). They are utilised in various artillery, tank, and aerial weapon systems. As essential components of modern ballistic systems, grenades are designed to precisely engage targets at varying distances. They are launched from weapon platforms, including cannons, howitzers, rocket systems, and handheld grenade launchers. Additionally, infantry units employ grenades using rifles equipped with grenade launchers, typically of 40 mm calibre (Hrvatska enciklopedija, 2025). The primary purpose of grenades is the neutralisation of targets at long ranges, which may include military infrastructure, equipment, transportation and communication hubs, as well as personnel.

A grenade consists of several key components (Figure 1), each with a specific function in its effectiveness and safety. All components are designed and manufactured to function together to ensure reliability, efficiency, and safety in military operations.

Figure 1
Cross-section of an impact grenade

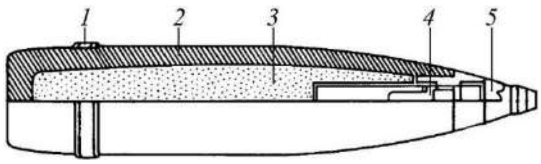

Note. 1. driving band, 2. body (casing), 3. explosive charge, 4. detonator, 5. Fuse. Source: Hrvatska enciklopedija, 2025

For the purpose of describing projectile flight, a model with six degrees of freedom (6DOF) is often selected, as referenced in the literature (Janković et al., 1999), (Gkritzapis et al., 2007). This model fully describes both the motion of the centre of mass and the motion around the centre of mass. A less complex but also less accurate model, the Modified Point Mass Model (MPMM), which has four degrees of freedom, is not applicable to all projectile classes and has proven particularly unsuitable for modelling the flight of reactive projectiles during the active phase of flight (Corriveau, 2017).

The aforementioned 6DOF models are primarily developed in the body-fixed coordinate system (F-CS) or its non-rotating variant, the aeroballistics coordinate system (B-CS) (Janković, 1998). However, neither of these coordinate systems is suitable for describing the flight of an asymmetric projectile. Therefore, a new version of the 6DOF flight model is being developed within the previously introduced geometric coordinate system (G-CS) (Trzun et al., 2021). To emphasize its distinction from the classical 6DOF model, this model will be referred to as G6DOF.

The governing equations of the G6DOF model are derived from:

1. A modified form of Newton's law for bodies with variable mass m, according to which the derivative of flight velocity V_K^G is equal to the vector sum of the aerodynamic force F_A^G, the thrust or reactive force F_T^G, and the gravitational force mg^G. Due to the principle of solidification, mass is not differentiated. All forces are expressed in the G-CS. Since we consider the derivative in the relative coordinate system G-CS, which is fixed to the rocket, the Coriolis inertial force ma_{cor}^G is also included:

$$m(\dot{V}_K^G + \tilde{\Omega}_G \cdot V_K^G) = F_A^G + F_T^G + L_{GO} m g^O - m a_{cor}^G \tag{1}$$

2. The derivative of the kinetic moment of a body with variable mass, which is equal to the sum of the moment of the aerodynamic force M_A^G and the moment of the thrust force M_T^G:

$$\dot{H}^G + \tilde{\Omega}_G \cdot H^G = M_A^G + M_T^G, \tag{2}$$

where the kinetic moment H^G is equal to the product of the inertia tensor in the G-CS (since we seek the components of the kinetic moment in this coordinate system) and the angular velocity of the rocket, which is equal to the angular velocity of the G-CS: $H^G = I^G \Omega_G^G$. $\dot{H}^G$ represents the derivative of the components of the kinetic moment vector.

3. The matrix form of the kinematic equation, which links the projectile's orientation $s^G = [\varphi_G \; \vartheta_G \; \psi_G]^T$ to the angular velocity of the G-CS $\Omega_G^G = [p \; q \; r]^T$:

$$\dot{s}^G = R^{-1}(\varphi, \vartheta) \cdot (\Omega_G^G - \Omega_O^G), \tag{3}$$

where Ω_O^G is the angular velocity matrix of the transported coordinate system, and R is defined as

$$R = \begin{bmatrix} 1 & 0 & -\sin\vartheta_G \\ 0 & \cos\varphi_G & \sin\varphi_G \cos\vartheta_G \\ 0 & -\sin\varphi_G & \cos\varphi_G \cos\vartheta_G \end{bmatrix} \tag{4}$$

4. The relationship between velocity and the derivatives of coordinates in the geocentric coordinate system (E-CS):

$$\begin{gathered} V_{Kx}^O = \dot{\varphi}_E (R_E + h) \\ V_{Ky}^O = (\dot{\lambda} + \Omega_E) \cdot (R_E + h) \, cos \, \varphi_E \\ V_{Kz}^O = -\dot{h}, \end{gathered} \tag{5}$$

where h is the altitude above sea level, R_E is the Earth's radius, and Ω_E is its angular velocity; φ_E and λ represent the geographic latitude and longitude, respectively.

By applying the aforementioned system of governing equations, a state vector is obtained with the following unknowns, or components:

$$\boldsymbol{X} = \begin{bmatrix} \varphi_E & \lambda & h & \underbrace{u_K \quad v_K \quad w_K}_{\boldsymbol{V}_K^G} & \underbrace{H_x \quad H_y \quad H_z}_{\boldsymbol{H}^G} & \underbrace{\varphi_G \quad \vartheta_G \quad \psi_G}_{\boldsymbol{s}^G} \end{bmatrix}^T$$

The development of the governing equations (1)–(5) leads to a system of twelve equations, representing the so-called "classical" 6DOF model.:

$$\begin{bmatrix} \dot{x} \\ \dot{z} \\ \dot{Z} \end{bmatrix} = \boldsymbol{L}_{LP} \begin{bmatrix} u_k \\ \tilde{v}_k \\ \tilde{w}_k \end{bmatrix}$$

$$\dot{u}_k = -\tilde{q}\tilde{w}_k + \tilde{r}\tilde{v}_k + \frac{X + F_x}{m} - g \sin\vartheta - a_{Kx}$$

$$\dot{\tilde{v}}_k = p_P \tilde{w}_k - \tilde{r} u_k + \frac{\tilde{Y} + F_{\tilde{y}}}{m} - a_{K\tilde{z}}$$

$$\dot{\tilde{w}}_k = -p_P \tilde{v}_k + \tilde{q} u_k + \frac{\tilde{Z} + F_{\tilde{z}}}{m} + g \cos\vartheta - a_{K\tilde{z}}$$

$$\dot{p} = \frac{(L + L^F)}{I_x}$$

$$\dot{\tilde{q}} = p_P \tilde{r} + \frac{-I_x p \tilde{r} + \tilde{M} + \tilde{M}^F}{I_y}$$

$$\dot{\tilde{r}} = -p_{PA} \tilde{q} + \frac{I_x p \tilde{q} + \tilde{N} + \tilde{N}^F}{I_y}$$

$$\dot{\varphi} = p + \tilde{r} tg\vartheta$$

$$\dot{\vartheta} = \tilde{q}$$

$$\dot{\psi} = \frac{\tilde{r}}{\cos\vartheta}$$

In the equations for the derivatives of the flight velocity components of the projectile (u_k, v_k, w_k), the components of the aerodynamic force $\vec{F}$ appear, which directly depend on the projectile's frictional drag. Similarly, in the equations for the derivatives of the angular velocities, the aerodynamic moment $\vec{M}$, appears, which is also dependent on the friction coefficient, which in turn directly depends on the quality of the surface treatment.

The surface treatment of a grenade is of critical importance as it directly influences its mechanical, tribological, and ballistic properties. While most attention in grenade design is typically focused on its internal structure, explosive charge, and activation mechanisms, the quality of the external surface also plays a key role in its functionality and longevity. Surface roughness, which refers to microstructural irregularities on the outer layers of the grenade, can significantly impact its performance during various stages of use, including force delivery upon firing, interaction with the target, and long-term resistance to damage and erosion during storage and operation.

The surface topography of the grenade casing can affect mechanical integrity and failure mechanisms during detonation. For instance, microtextures or specific surface treatments can enhance the fatigue resistance of materials used in grenade construction. Research has shown that surface roughness influences material fatigue behaviour, with smoother surfaces generally demonstrating superior fatigue performance compared to rougher ones (Demeneghi et al., 2025). Surface roughness can also affect the mechanism of impact force detection during the explosion, as surface irregularities may alter how forces propagate through the material. Such irregularities can create microscopic stresses that may accelerate the initiation of cracks or damage due to mechanical impacts.

Tribology, which studies friction, wear, and lubrication, also plays a crucial role in the performance of grenades. During their use, grenades come into contact with various surfaces, including gun barrels, targets, and other weapon components. Surface roughness can significantly influence the tribological characteristics of a grenade, particularly in the context of reducing friction during firing and increasing durability for repeated use. For example:

- Grenades with high surface roughness may exhibit a higher coefficient of friction, leading to increased wear on firearm systems and barrels, thereby reducing efficiency and extending weapon maintenance intervals (Bisyk, 2021).
- Smooth surfaces can reduce friction, decreasing mechanical stress during firing and potentially improving grenade accuracy. However, they may also necessitate additional protective coatings to prevent damage from exposure to high temperatures or highly abrasive environmental materials (Bisyk, 2021).

Moreover, surface roughness can significantly affect the interaction between the grenade and its environment, particularly in friction and wear (Ali et al., 2023). Surface roughness also influences the ballistic properties of grenades, particularly their aerodynamics and flight precision. In some cases, increased roughness can enhance air turbulence around the grenade, negatively impacting its stability and accuracy. Reducing roughness or polishing the surface can improve flight stability, minimising vibration and lateral deviations during air travel (Elkilany et al., 2019).

Roughness also significantly impacts the grenade's long-term performance, including its resistance to corrosion and wear. Surface layers containing roughness can accumulate water and other corrosive substances, which may reduce the material's durability and lead to faster degradation. Surface treatments such as anodising or plastic coatings can significantly reduce the risk of corrosion and enhance the grenade's durability during storage and prolonged use. The surface topography analysis is crucial for understanding the material's microstructural characteristics, including roughness, irregularities, microscopic pores, and other features that can significantly influence the material's performance under real-world conditions.

2. MATERIALS AND METHODS

2.1. Sample description

In this study, parts of the grenade casing were analysed, with different types of surface treatments selected to assess their impact on surface topography. All examined samples were made from an aluminium alloy, commonly used in grenade construction due to its low mass, high specific strength, and corrosion resistance. Aluminium alloys enable good ballistic performance while optimising the projectile's weight, which affects its range and flight stability.

Surface topography comparison was conducted on test samples with various treatments:

1. Plastic-coated sample – The surface is covered with a protective polymer coating layer. This treatment is applied to protect against corrosion and reduce friction. A lower roughness is expected compared to anodised samples, although variations may occur depending on the thickness and uniformity of the coating.
2. Anodised sample – The surface was subjected to anodisation, an electrochemical process that forms an oxide layer on aluminium. This layer increases corrosion resistance and may improve the adhesion of protective coatings. A moderate roughness is expected, as anodisation can form a microporous structure.
3. Hard-anodised sample—This is similar to standard anodisation, but the process was conducted at lower temperatures and higher voltages, creating a thicker and harder oxide layer. This treatment improves wear resistance, thereby extending the grenade's service life. Increased roughness is expected due to developing a more pronounced microporous and micro-relief structure, which may affect friction and ballistic properties.

Figure 2 shows the analysed measurement samples.

Figure 2. Measured samples

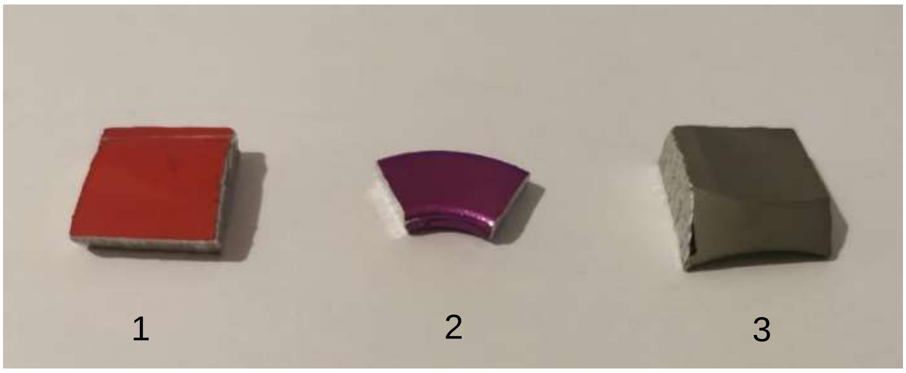

Note. 1 – Plastic coated, 2 – Anodised, 3 – Hard anodised

2.2. Atomic force microscopy (AFM)

Atomic force microscopy (AFM) enables surface topography analysis at the nanometre scale. AFM uses the mechanical interaction between the probe tip (typically made of silicon or silicon nitride) and the sample surface to map surface topography characteristics. In AFM, the probe is attached to the cantilever. As the probe moves across the sample surface, atomic forces (van der Waals forces) interact, causing the cantilever to bend. These changes are recorded by a laser system and photodetector, which translates them into a surface topography map (Razumić et al., 2024).

AFM can operate in several modes, but for surface topography analysis, the most commonly used are:

- Contact Mode – The probe constantly touches the surface and follows its irregularities.
- Tapping Mode – The probe oscillates near the resonant frequency and gently taps the surface at regular intervals, reducing the risk of damaging sensitive samples.

Atomic force microscopy measurements provide areal topography parameters, which are also referred to in the literature as 3D topography parameters.

2.3. Areal Topography Parameters

According to the ISO 25178-2:2021 standard, Geometrical Product Specifications – Surface Texture: Area – Part 2: Terms, Definitions, and Surface Texture Parameters (*ISO 25178-2:2021(En), Geometrical Product Specifications (GPS) — Surface Texture: Areal — Part 2: Terms, Definitions and Surface Texture Parameters*) (ISO, 2021), areal topography parameters are divided into five main groups: amplitude, spatial, hybrid, functional, and miscellaneous. In this study, amplitude areal topography parameters were analysed. A description and formulas for calculating the areal topography parameters are provided in Table 1.

Table 1. Amplitude areal topography parameters

Parameter	Description	Formula	What does it measure?	Type of information
Sa (arithmetic mean height)	Average absolute height of the profile	$Sa = \sqrt{\frac{1}{A}\iint_A \lvert z(x,y)\rvert dxdy}$	Average surface roughness.	Mean height value
Sq (root mean square height)	Standard deviation of height	$Sq = \sqrt{\frac{1}{A}\iint_A z^2(x,y)dxdy}$	Similar to *Sa*, but more sensitive to extremes	Height dispersion

Sz (maximum height of the surface)	Difference between the highest and lowest points	$Sz = Sp + Sv$	Total surface range	Extreme values
Sp (maximum peak height)	Highest point above the mean plane		Most prominent peaks	Extreme values
Sv (maximum valley depth)	Lowest point below the mean plane		Deepest valleys	Extreme values
Ssk (Skewness)	Asymmetry of height distribution	$Ssk = \frac{1}{Sq^3}\left[\frac{1}{A}\iint_A z^3(x,y)dxdy\right]$	Dominance of peaks/valleys	Distribution shape
Sku (Kurtosis)	Sharpness of peaks and depth of valleys	$Sku = \frac{1}{Sq^4}\left[\frac{1}{A}\iint_A z^4(x,y)\,dxdy\right]$	Excess of extreme values	Distribution shape

3. RESULTS AND DISCUSSION

The measurements of the samples were conducted using an *Oxford MFP-3D Origin* atomic force microscope in tapping mode, at three measurement points on each sample. The input scanning parameters were as follows:

- Scan size: 10 µm × 10 µm
- Scan resolution: 256
- Scan speed: 12.5 µm s^{-1}

Surface topography images, in both 2D and 3D formats, obtained with the AFM are shown in Figure 3, where:

1 – Plastic-coated sample
2 – Anodised sample
3 – Hard anodised sample.

Figure 3. Surface topography appearance for samples 1 – 3

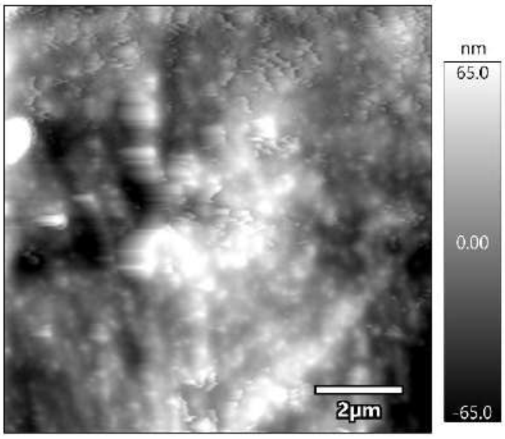

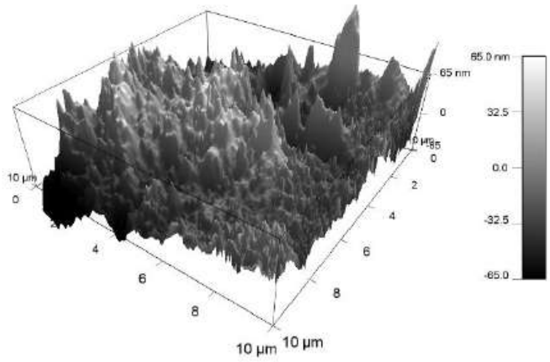

1.a) 1.b)

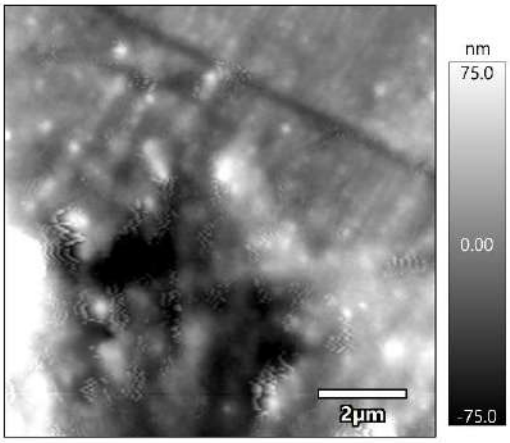

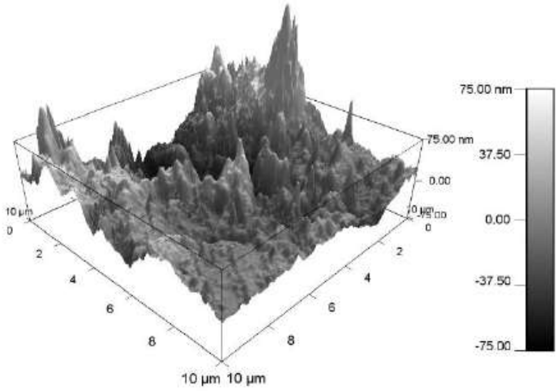

2.a) 2.b)

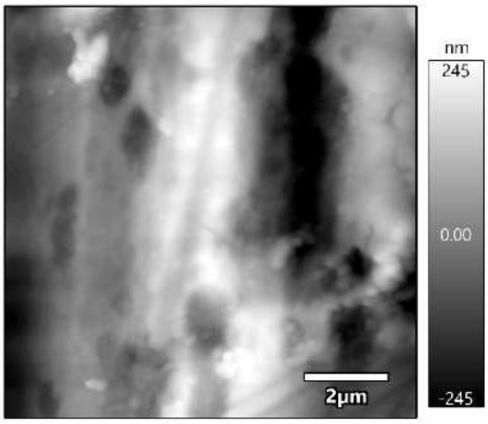

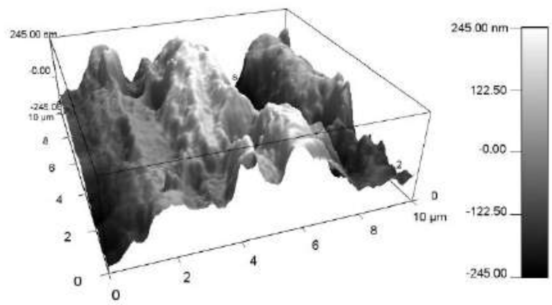

3.a) 3.b)

The measurement results of the areal topography parameters are provided in Table 2.

Table 2. Areal topography parameters

Sample No.	Measurement point	*Sq*/nm	*Sa*/nm	*Sz*/nm	*Sp*/nm	*Sv*/nm	*Ssk*/-	*Sku*/-
1	1	31.374	24.736	272.452	139.906	132.546	0.168	3.490
	2	36.238	27.640	294.212	151.327	142.885	0.146	3.891
	3	48.836	39.869	308.699	168.995	139.704	0.279	2.758
	$\bar{x}$	38.816	30.748	291.788	153.409	138.378	0.198	3.380
	s	9.012	8.031	18.245	14.656	5.295	0.071	0.575
2	1	37.858	26.550	390.623	237.028	153.595	0.892	7.250
	2	58.187	44.834	452.077	250.043	202.034	0.333	3.847
	3	50.521	38.025	437.610	270.085	167.525	0.955	5.510
	$\bar{x}$	48.855	36.470	426.770	252.385	174.385	0.727	5.536
	s	10.266	9.241	32.129	16.653	24.937	0.342	1.702
3	1	117.714	92.926	968.916	406.064	562.852	-0.420	3.662
	2	237.817	188.258	1527.488	582.009	945.479	-0.142	3.800
	3	213.399	164.699	1357.458	653.885	703.573	-0.592	3.597
	$\bar{x}$	189.643	148.628	1284.621	547.319	737.301	-0.385	3.686
	s	63.478	49.656	286.321	127.500	193.531	0.227	0.104

Figure 4 shows the arithmetic means of the measured parameters' values.

Figure 4. Arithmetic means of amplitude topography parameters depending on the sample

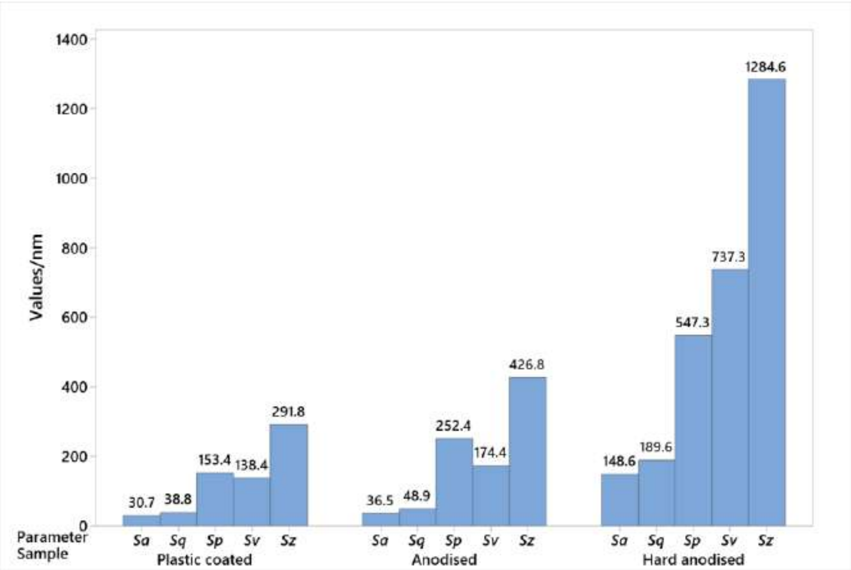

Note. The values are expressed in nm (*Sa*, *Sq*, *Sp*, *Sv*, and *Sz*).

Table 1 and Figure 4 show that the plastic-coated surface has the lowest values of the topography parameters, indicating a relatively smooth surface. The standard deviation is the smallest, which suggests a uniform finish. The anodised surface has higher values compared to the plastic-coated surface. The hard-anodised surface has the highest values for all parameters (*Sa* = 148.63 nm, *Sq* = 189.64 nm, *Sz* = 1284.62 nm), indicating a highly rough surface. This treatment is known for its high wear resistance; however, increased roughness may negatively affect aerodynamic characteristics. The *Sp*, *Sv*, and *Sz* parameters are the smallest for the plastic-coated sample, meaning that the plastic-coated sample has no pronounced irregularities. The decorative anodised surface has higher values for the *Sp*, *Sv*, and *Sz* parameters, which may indicate better adhesion of protective layers. The hard-anodised sample shows extreme values for *Sp* (547.32 nm) and *Sv* (737.30 nm).

The *Ssk* and *Sku* parameters describe the shape of the surface topography distribution. The plastic-coated surface has *Ssk* = 0.198, suggesting a symmetrical distribution of peaks and valleys. *Sku* = 3.38, indicating slightly rounded peaks. The decorative anodised surface has *Ssk* = 0.727, meaning the surface contains more sharp peaks than valleys. *Sku* = 5.54, confirming the presence of more pronounced sharp peaks. The hard-anodised surface shows a negative *Ssk* = –0.385, indicating that the surface has more profound valleys than peaks. *Sku* = 3.69, suggesting a relatively uniform distribution of peaks and valleys, but with more pronounced indentations.

To investigate the effect of different surface finishes on surface topography, an analysis of variance (ANOVA method) and Fisher Least Significant Difference (LSD) *t*-test were performed. In the Fisher *t*-test, the corresponding means are significantly different if an interval does not contain zero. The significance level of the test was set to $\alpha = 0.05$. The results of the statistical tests are presented in Table 3.

Table 3. ANOVA: p-values

Parameter	*p*-value
Sa	0.004
Sz	0.001
Sq	0.004
Sp	0.002
Sv	0.001
Ssk	0.004
Sku	0.087

The *p*-values from Table 3 show that, for all areal topography parameters except for the *Sku* parameter, which indicates the sharpness of the profile, there is sufficient evidence to conclude that the surface topography of the tested samples is statistically different. The 95% confidence intervals for the conducted analysis of variance and Fisher's *t*-test are shown in Figure 5.

Figure 5. The 95% confidence interval (left) and Fisher's t-test (right)

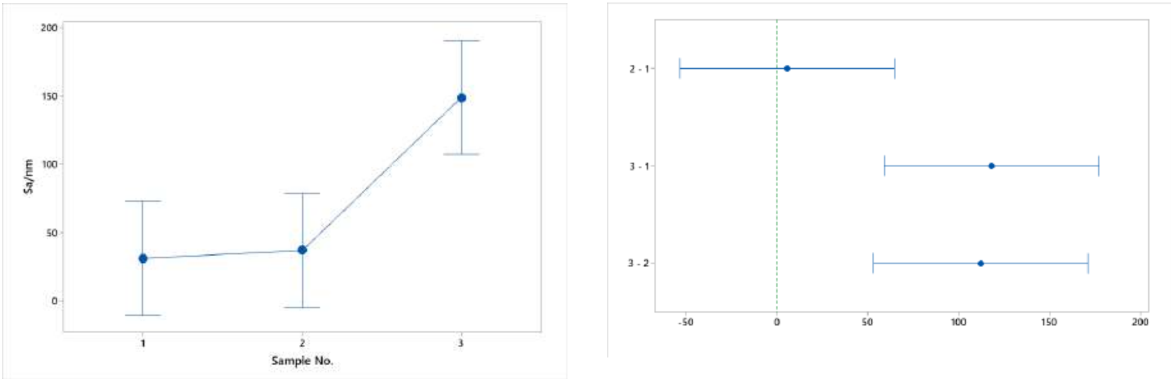

a) parameter *Sa*

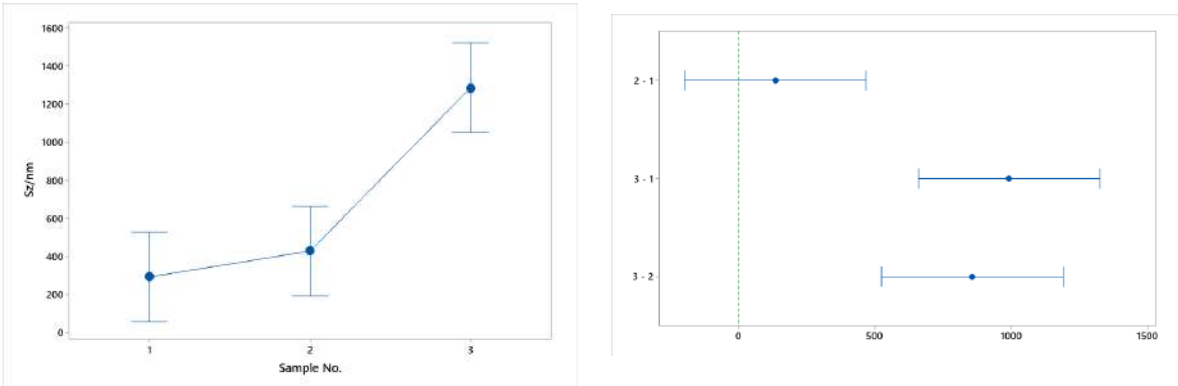

b) parameter *Sz*

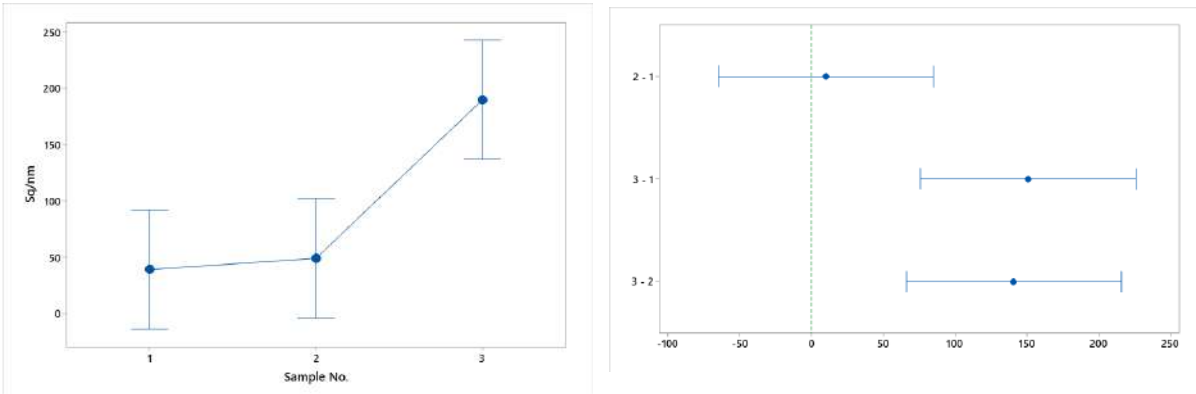

c) parameter *Sq*

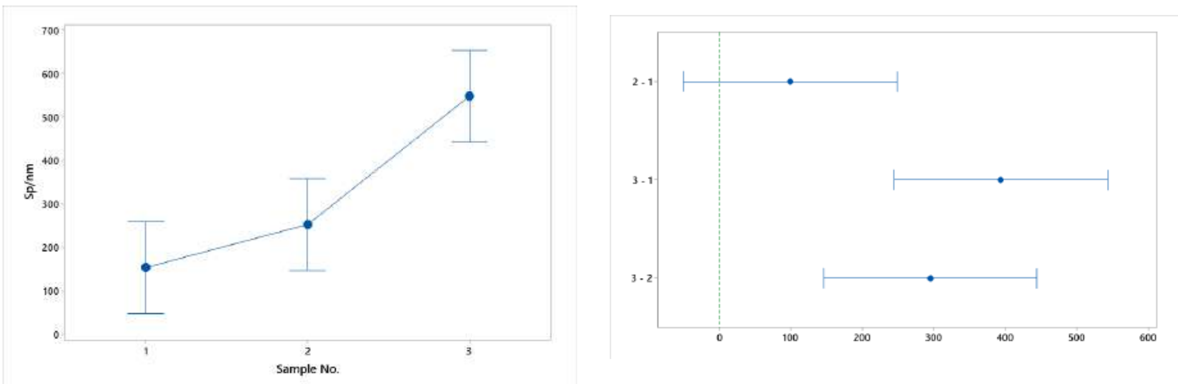

d) parameter *Sp*

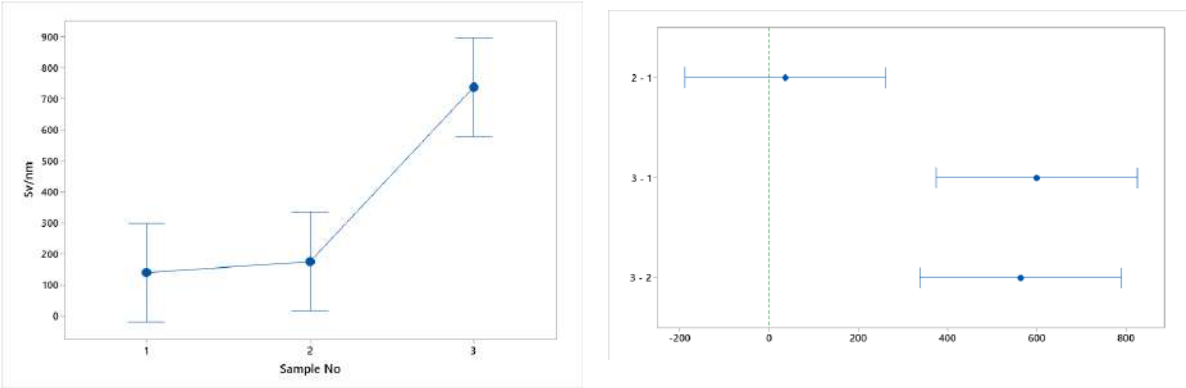

e) parameter *Sv*

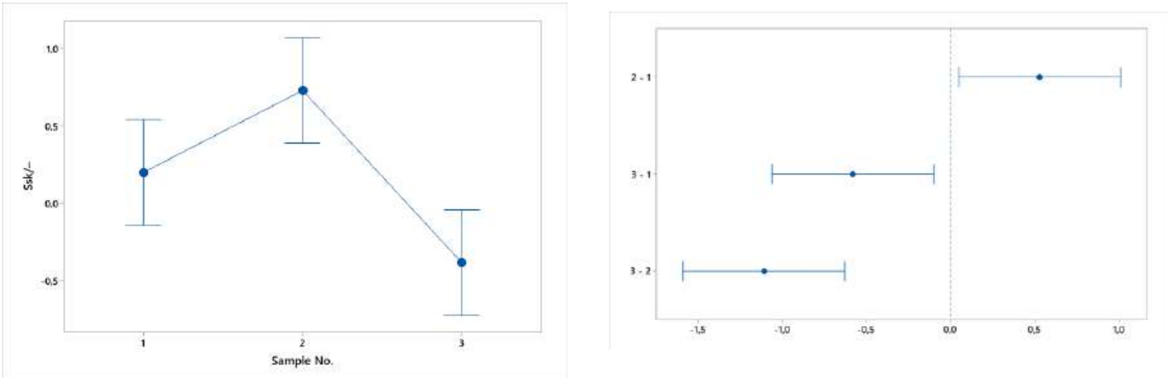

f) parameter *Ssk*

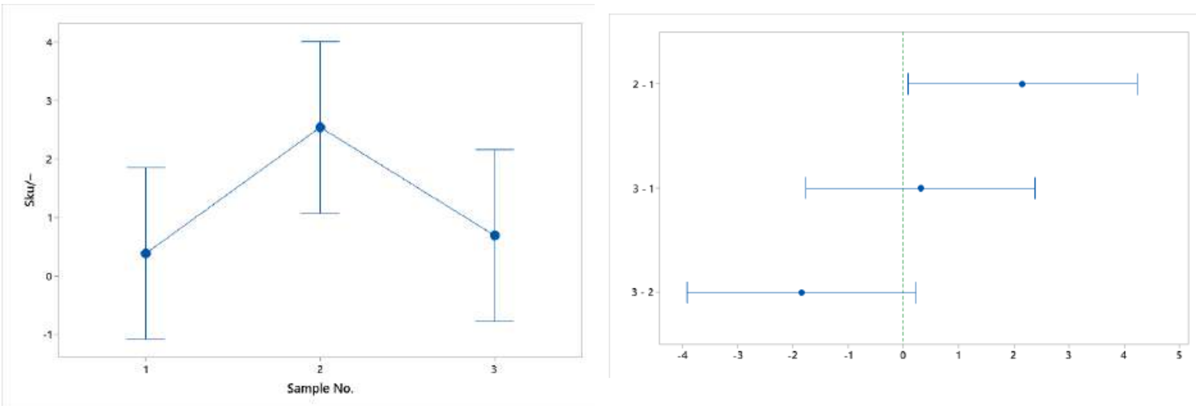

g) parameter *Sku*

For the amplitude areal topography parameters that directly measure the height values of the topography parameters and are expressed in the unit of measurement nm (*Sa*, *Sq*, *Sz*, *Sp*, and *Sv*), there is a statistically significant difference between sample 3 (hard anodised) and both sample 1 (plastic coated) and sample 2 (anodised). There is insufficient evidence for samples 1 and 2 to conclude that their surface topographies are statistically significantly different.

The following information is obtained by performing the variance analysis for the parameters that describe the shape of the height distribution (Ssk and Sku): the distribution of peaks and valleys is different for all three samples (parameter *Ssk*). The analysis of variance showed no statistically significant difference between the samples for the *Sku* parameter. However, Fisher's test showed a statistical difference between sample 1 and sample 2.

4. CONCLUSION

This study demonstrated the impact of different surface treatments on the topography of grenade shell casings using Atomic Force Microscopy. The results revealed significant differences in the topography between plastic-coated, anodised, and hard-anodised samples:

- The plastic-coated surface exhibited the lowest roughness (Sa = 30.75 nm, Sq = 38.82 nm, Sz = 291.79 nm), indicating a smooth and homogeneous structure suitable for reducing friction and improving aerodynamic properties.
- The anodised surface showed a moderate increase in roughness (Sa = 36.47 nm, Sz = 426.77 nm) with more pronounced peaks, which may enhance wear resistance and coating adhesion.
- The hard anodised surface had extremely high roughness (Sa = 148.63 nm, Sz = 1284.62 nm), suggesting more excellent mechanical resistance and increased friction and potential aerodynamic losses.
- Using the ANOVA method and Fisher's *t*-test, no statistically significant differences were found between the plastic-coated and anodised samples. Statistically significant differences were observed when comparing the complex anodised sample with the plastic-coated and anodised samples.

The choice of the best surface treatment depends on the specific application – if aerodynamics and friction reduction are priorities, the plastic-coated surface offers the best performance. At the same time, anodised coatings help enhance mechanical resistance and material durability. Plastic coating can benefit projectiles where reducing air resistance and improving accuracy are critical. Anodising can strike a balance between wear resistance and aerodynamic properties. Hard anodising can enhance the mechanical durability of projectiles, particularly under high wear or pressure conditions. Implementing these findings can lead to longer-lasting, more precise, and more efficient projectiles tailored to specific mission requirements. Suggestions for future research aimed at optimising the production and performance of modern grenades, adapting surface treatments to specific tactical and technical requirements:

- Experimental analysis of friction and wear on different surfaces under actual firing conditions.
- Investigation of aerodynamic effects of various topographies to quantify the impact of roughness on flight accuracy.
- Electrochemical testing of corrosion phenomena on grenade shell casing surfaces.

5. REFERENCES

Ali, S., Kurniawan, R., Chul, P. G., & Ko, T. J. (2023). Tribological properties of hierarchical micro-dimples produced on a cylindrical surface by dual-frequency texturing. *Friction, 11*(2), 246–258. https://doi.org/10.1007/s40544-022-0598-5

Bisyk, S. (2021). Investigation of the RPG grenade warhead interaction with the slat armor. https://doi.org/10.36074/logos-15.10.2021.10

Corriveau, D. (2017). Validation of the NATO Armaments Ballistic Kernel for use in small-arms fire control systems. *Defence Technology, 13*(3), 188–199. https://doi.org/10.1016/j.dt.2017.04.006

Demeneghi, G., Gradl, P., Diaz, A., & Hazeli, K. (2025). Effect of surface finish and temperature on low cycle fatigue behavior of GRCop-42. *Fatigue & Fracture of Engineering Materials & Structures, 48*(2), 840–856. https://doi.org/10.1111/ffe.14526

Elkilany, H. A., Shoeib, M. A., & Abdel-Salam, O. E. (2019). Influence of hard anodizing on the mechanical and corrosion properties of different aluminum alloys. *Metallography, Microstructure, and Analysis, 8*(6), 861–870. https://doi.org/10.1007/s13632-019-00594-5

Gkritzapis, D. N., Panagiotopoulos, E. E., Margaris, D. P., Papanikas, D. G., Simos, T. E., & Maroulis, G. (2007). A six-degree-of-freedom trajectory analysis of spin-stabilized projectiles. In *AIP Conference Proceedings* (pp. 1187–1194). AIP. https://doi.org/10.1063/1.2835958

Hrvatska enciklopedija. (2025). Granata. *Hrvatska enciklopedija*. Accessed: Feb. 09, 2025. Available: https://www.enciklopedija.hr/

ISO (2021). *ISO 25178-2:2021(en), Geometrical product specifications (GPS) — Surface texture: Areal — Part 2: Terms, definitions and surface texture parameters*. International Organization for Standardization. https://www.iso.org/obp/ui/#iso:std:iso:25178:-2:ed-2:v1:en:fig:7

Janković, S. (1998). *Mehanika leta projektila*. Zagreb: Faculty of Mechanical Engineering and Naval Architecture.

Janković, S., Gallant, J., & Celens, E. (1999). Dispersion of an artillery projectile due to unbalance. *Proceedings - 18th International Symposium on Ballistics, 1*, 128–141.

Razumić, A., Runje, B., Lisjak, D., Kolar, D., Horvatić Novak, A., Štrbac, B., & Savković, B. (2024). Atomic force microscopy: Step height measurement uncertainty evaluation. *Tehnički glasnik, 18*(2), 209–214. https://doi.org/10.31803/tg-20230829155921

Trzun, Z., Vrdoljak, M., & Cajner, H. (2021). The effect of manufacturing quality on rocket precision. *Aerospace, 8*(6), 160. https://doi.org/10.3390/aerospace8060160